KSCE Journal of Civil Engineering (0000) 00(0):1-17
DOI 10.1007/s12205-013-0689-y

Structural Engineering
pISSN 1226-7988, eISSN 1976-3808
www.springer.com/12205

Experimental and FE Study on RC One-Way Slabs Upgraded with FRP Composites

Hussein M. Elsanadedy*, Tarek H. Almusallam, Saleh H. Alsayed***, and Yousef A. AL-Salloum******

Received November 19, 2013/Revised March 2, 2014/Accepted April 28, 2014/Published Online October 17, 2014

Abstract

The use of externally bonded Fiber Reinforced Polymer (FRP) composites as a means of upgrading the flexural capacity of Reinforced Concrete (RC) one-way slabs is experimentally and numerically investigated in this study. A total of four groups of eight slabs were tested under four-point bending. The two slabs of the first group were left unstrengthened to be used as control specimens. The two slabs of the second group were externally strengthened with adhesively bonded pultruded, pre-cured CFRP plates. The four slabs of the last two groups were externally upgraded with unidirectional carbon (or E-glass) fiber fabric impregnated with an epoxy resin. In addition to the experimental program, a numerical investigation utilizing nonlinear Finite Element (FE) analysis was conducted using LS-DYNA software. Besides the eight slabs tested in this study, another eleven slabs were collected from the literature for the purpose of finite element validation. A comparison was made between the experimental and numerical results and good agreement was achieved. Based on FE validation, the numerical analysis was extended to include additional cases to study the effect of axial FRP stiffness and FRP-to-concrete width ratio on the flexural performance of upgraded slabs. As a result of the numerical study, new stiffness and reinforcement parameters were introduced in this research. These parameters were employed in the development of two new formulas for predicting the FRP debonding strain and percent gain in flexural capacity of FRP-strengthened slabs.

Keywords: *fiber reinforced polymer, concrete one-way slabs, flexural strengthening, finite element modeling*

1. Introduction

Externally bonded Fiber Reinforced Polymer (FRP) composites are considered as effective means for rehabilitation of deficient Reinforced Concrete (RC) members (Meier, 1992; Norris *et al.*, 1997; Shahway *et al.,* 2001; Issa *et al.*, 2000; Issa *et al.*, 2003). Limited research studies are available reporting on repair and strengthening of one-way and two-way RC slabs with FRP composites, even though the problem of their upgrade, both in buildings and in bridges, is quite common. The latest studies and experience demonstrated that rehabilitation of RC slabs require less FRP material to achieve equivalent increases in stiffness and strength compared with RC beams (Erki and Heffernan, 1995; Seim *et al*., 2001; Tan 2003; Al-Rousan *et al*., 2012; Lesmana and Hu, 2014).

For FRP-upgraded flexural members, depending on the combination of parameters such as member size, steel reinforcement ratio, FRP properties and dimensions, etc., failure may occur in different modes (Meier, 1995; Arduini *et al.,* 1997; Buyukozturk and Hearing, 1998). The dominant failure mode is debonding of the FRP system. Debonding failure typically propagates within the concrete substrate. Sources of FRP debonding include local cracks in a host concrete member, degradation of FRP-concrete interface, and stress concentrations induced by FRP configurations and irregular concrete surface (Smith and Teng, 2001; Mazzotti *et al.*, 2008). Most FRP-debonding may be classified (Oehlers *et al.,* 2003) as either end debonding (also referred to as concrete cover delamination) or intermediate-crack-induced debonding (IC debonding henceforth). End debonding occurs due to the combination of normal and shear stresses at the termination point of FRP and propagates along the FRP. IC debonding is induced by a geometric discontinuity of a strengthened member at the location of flexural or shear/flexural cracks and propagates in the direction of decreasing moment. End debonding failure usually propagates at the level of the internal reinforcement (splitting-like failure), whereas IC debonding takes place within the cover concrete a few millimeters above the bond line. IC debonding limits the composite behavior and therefore influences the effectiveness of the FRP system. Local debonding failure propagates along the FRP-concrete interface zone with increased

*Assistant Professor, Specialty Units for Safety and Preservation of Structures, Dept. of Civil Eng., King Saud University, Riyadh 11421, Saudi Arabia (Corresponding Author, Email: elsanadedy@yahoo.com)
**Professor, Dept. of Civil Engineering, King Saud University, Riyadh 11421, Saudi Arabia (E-mail: musallam@ksu.edu.sa)
***Professor, Dept. of Civil Engineering, King Saud University, Riyadh 11421, Saudi Arabia (E-mail: shalsayed@gmail.com)
****Professor, Dept. of Civil Engineering, King Saud University, Riyadh 11421, Saudi Arabia (E-mail: ysalloum@ksu.edu.sa)

load. In practice, end debonding is rare, critical only in short, shear-dominated members, and is easily mitigated using anchorage (typically, FRP U-wraps) near the termination point of FRP. IC debonding is not easily controlled (Sebastian, 2001; Kim *et al.*, 2008) and therefore FRP stresses must be limited in order to mitigate it.

Arduini *et al.* (2004) studied experimentally the behavior of 26 full-scale one-way RC slabs strengthened with unidirectional Carbon Fiber-Reinforced Polymer (CFRP) laminates installed by manual wet lay-up. Twenty-six slabs with and without an overhang at one extremity were tested under simply supported conditions. The geometry and loading configuration allowed for the study of positive and negative moment regions. Different failure mechanisms-namely concrete shear, concrete crushing, CFRP rupture, and CFRP debonding-were obtained by varying the CFRP laminate cross-sectional area and the amount of internal steel reinforcement.

Seim *et al.* (2001) investigated experimentally the effect of prefabricated FRP strips and fabric on the behavior of RC one-way slabs. Thirteen slabs were tested to failure with varying configurations of FRP composites, while monitoring deflections, strains, and damage development. It is shown that, although the ultimate load level can be increased significantly, failure is associated with a drastically reduced deformation capability and a change from the conventional ductile mode of failure to a more brittle one. Tan (2003) conducted an experimental study on flexural strengthening of RC one-way slabs with different CFRP systems. Five simply supported slabs were tested to failure. The first specimen was used as the control slab. The second specimen was strengthened with 2 strips of adhesively bonded prefabricated CFRP plates. The third slab was strengthened with 2 strips of prestressed prefabricated CFRP plates. The fourth specimen was strengthened with one ply of manual lay-up carbon fiber sheet and the last slab was strengthened with 8 strips of Near Surface Mounted (NSM) CFRP bars. It is concluded that CFRP systems increased the flexural strength and reduced the deflections and crack widths of the strengthened slabs. The slab which was strengthened with NSM laminate bars exhibited the highest efficiency followed by prestressed prefabricated plates, manual wet lay-up laminate sheet, and lastly adhesively bonded CFRP plates.

In order to expand FRP utilization, conducting numerical studies is essential. Finite Element (FE) research on FRP-strengthened RC beams and slabs from the past decade has been reviewed and it was found that most researchers have not modeled the FRP-to-concrete interface (Mosallam and Mosalam, 2003; Hu *et al*., 2004; Santhakumar *et al.*, 2004; Lundquist *et al.,* 2005; Al-Rousan *et al*., 2012). However, only few studies have considered the effect of the interfacial behavior and successfully simulated the debonding failure modes (Aprile and Feo, 2007; Elsayed *et al*., 2007; Obaidat *et al*., 2010; Chen *et al.*, 2012; Lesmana and Hu, 2014).

Al-Rousan *et al.* (2012) tested eight RC one-way slabs strengthened with different layers and configurations of CFRP sheets. In addition, nonlinear FE analysis was conducted to simulate the behavior of the test specimens. In the FE models, full bond was assumed between steel bars and concrete and between CFRP layers and concrete substrate. The FE analysis was expanded to provide a parametric study of eighteen slabs that includes the effect of number of CFRP layers, contact area, and type of fiber on behavior of strengthened slabs. The experimental and FE results confirmed that strengthening of under-reinforced concrete slabs with CFRP improves the flexural strength capacity and reduces the ductility. Lesmana and Hu (2014) carried out nonlinear FE analysis to investigate the effect of slab thickness, concrete, steel bars and FRP properties on the behavior of FRP-strengthened RC two-way slabs. For FRP/concrete interface, two models were presented, fully bonded behavior and cohesive behavior. For the cohesive behavior, the interface between concrete and FRP was integrated to the model to simulate the bond behavior of the FRP composite. Perfect bond was assumed between steel bars and concrete. The FE model was validated using the test results of RC two-way slabs available in the literature. It is shown that the FE results for the fully bonded assumption are too stiff compared to the results that include interface modeling. It is concluded that the flexural capacity gain due to FRP strengthening is more significant when the slabs have lower steel ratio.

A search of literature has revealed numerous experimental studies on flexural strengthening of RC slabs using FRP composites. However, only a limited number of studies are available on the numerical modeling. The work done by Elsayed *et al.* (2007) and Lesmana and Hu (2014) focused on FE modeling of the FRP-to-concrete interfacial behavior in FRP-strengthened two-way slabs. In fact, a numerical study that considers the interfacial behavior between the FRP laminates and the concrete substrate and successfully simulates the debonding failure modes of FRP-strengthened one-way slabs could not be found. The lack of such research creates a challenge for the investigation of numerical modeling using the FE method, despite FE being an efficient and cost-effective numerical tool to model the structural behavior of RC members.

In this study, three different FRP composite systems were used to externally strengthen RC one-way slabs in flexure. A total of four groups of eight slabs were tested under four-point bending. In addition to the experimental program, numerical investigation was also carried out. The novelty of this study is that nonlinear FE analysis was conducted to predict the behavior of FRP-strengthened one-way slabs with the inclusion of FRP-to-concrete contact modeling, which would simulate the debonding failure modes. The developed FE models were validated using the experimental results of the eight specimens tested in this study in addition to eleven slabs tested by other researchers. Based on the validation of results, the numerical analysis was protracted to include additional cases to study the effect of axial FRP stiffness and FRP-to-concrete width ratio on the flexural performance of FRP-upgraded slabs.

2. Experimental Program

2.1 Test Matrix

The test matrix was designed to investigate the viability of using FRP composites in upgrading the flexural load capacity of RC one-way slabs. The test program consisted of 8 slabs divided into 4 groups consisting of two repeated slabs each. Specimens were duplicated to verify the repeatability of the results and to get more confidence in the conclusions of this study. All slab specimens were 1080 mm long with an effective span of 930 mm, 2010 mm wide, and 100 mm deep. The slab dimensions were selected to comply with available resources in the laboratory. With a concrete clear cover of 20 mm, all specimens were longitudinally reinforced with 8 Ø10 mm steel bars at 250 mm spacing resulting in a reinforcement ratio of 0.42%; whereas, 4 Ø8 mm steel bars at 300 mm spacing were placed in the transverse direction. All slab sections were intentionally designed to be under-reinforced to ensure flexural failure modes initiated by yielding of main tension steel, and to reveal the effectiveness of FRP composites in enhancing the flexural capacity. Two slabs (the first group "SC") were used as control specimens; whereas, the remaining 6 slabs (groups "SCP", "SCS" and "SGS") were externally strengthened in flexure with FRP composites. The main parameters studied experimentally were type of FRP system and axial FRP stiffness. Three different FRP systems with three axial stiffness values were investigated. Detailing and dimensions of test slabs are presented in Fig. 1. The test matrix is summarized in Table 1. It should be noted that in the design of FRP schemes for strengthened specimens, the general guidelines of Section

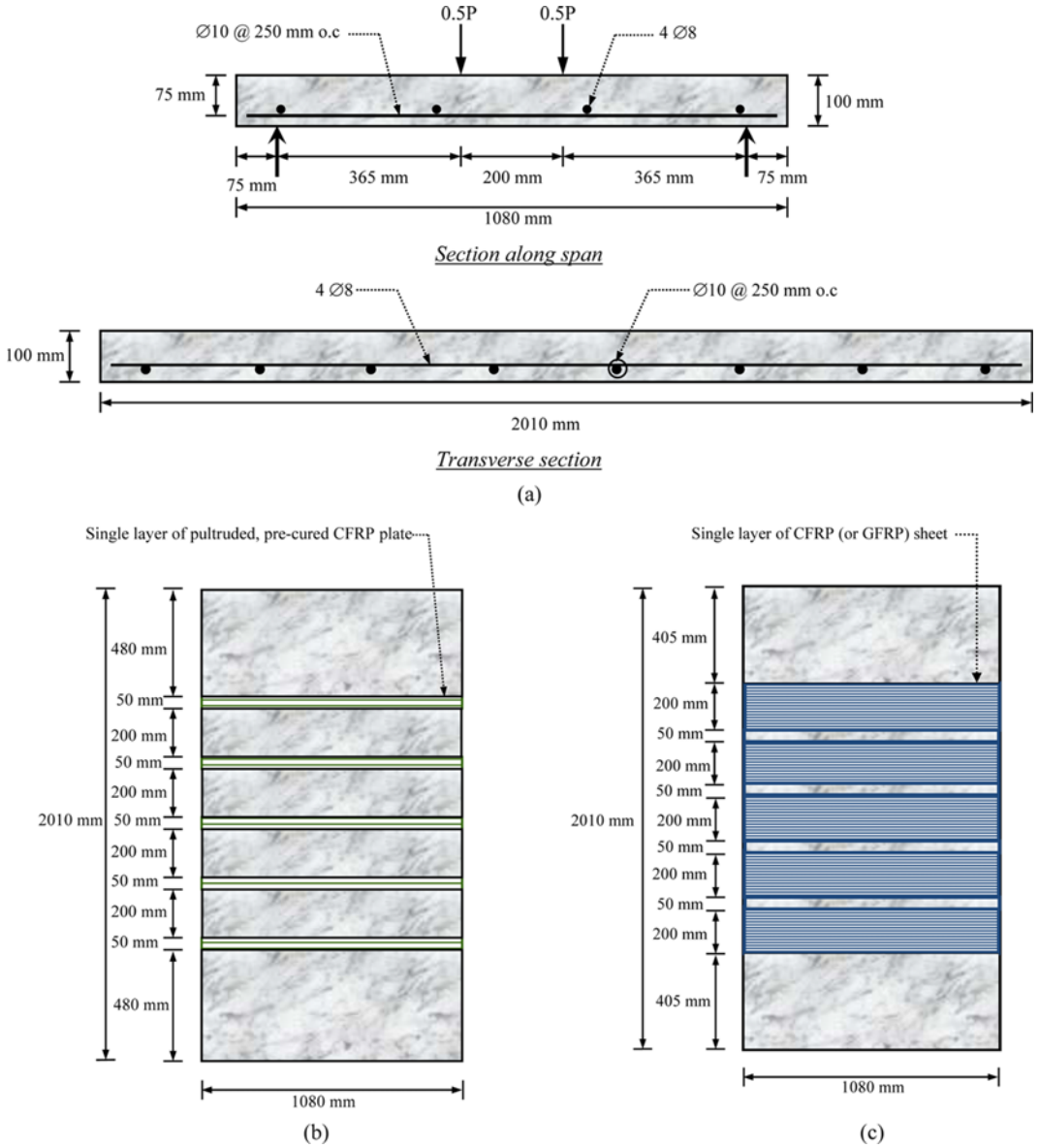

Fig. 1. Details of Test Slabs: (a) Control Specimen SC, (b) Strengthened Specimen SCP – Bottom View, (c) Strengthened Specimens SCS & SGS – Bottom View

Table 1. Test Matrix

Slab ID	Strengthening system	No. of specimens
SC	Control slab	2
SCP	Slabs strengthened with single layer of pultruded, pre-cured CFRP plate (5 strips, each 50 mm wide and 1080 mm long)	2
SCS	Slabs strengthened with single layer of CFRP sheet (5 strips, each 200 mm wide and 1080 mm long)	2
SGS	Slabs strengthened with single layer of GFRP sheet (5 strips, each 200 mm wide and 1080 mm long)	2
Total No. of specimens		8

13.1.2 of the ACI 440.2R-08 (ACI Committee 440, 2008) for the location of cutoff points for the FRP laminates were used to avoid end debonding failure mode. As per the guidelines, for simply supported members, a single-ply FRP laminate should be terminated at least a distance equal to l_{df} (development length as given by Eq. (13-2) of the ACI 440.2R-08) past the point along the span corresponding to the cracking moment. Thus, and due to the limited shear span of test specimens (only 0.365 m), the FRP laminates were extended to the end of the specimens as shown in Fig. 1.

2.2 Properties of Materials

2.2.1 Concrete and Steel Reinforcement

Ready-mix concrete was used to cast the slab specimens. Six standard cylinders (150×300 mm) were also prepared for compression testing at 28 days. The average compressive strength of the six cylindrical samples of the concrete mix was 24 MPa. For steel reinforcement, it should be noted that Ø8 mm Ø10 mm bars were made of mild and high strength steel, respectively. In order to determine the actual characteristics of steel reinforcement, three samples of steel bars from each diameter were tested under tension. The average values for yield strength of Ø8 and Ø10 mm steel bars are 240 and 528 MPa, respectively. The average values for tensile strength of Ø8 and Ø10 mm steel bars are 372 and 690 MPa, respectively.

2.2.2 FRP Composite Systems

Three commercially available FRP composite systems were

Table 2. Material Properties used in the FE Modeling of Slabs Tested in this Study

Concrete			
Material model	MAT_CSCM_CONCRETE		
Density (kg/m^3)	2320		
Uni-axial compressive strength (MPa)	24.0		
Max aggregate size (mm)	10		
Erosion criteria	5% Maximum principal strain		
Steel bars			
	Ø10 main tension steel bars	Ø8 shrinkage & temperature bars	
Material model	MAT_PIECEWISE_LINEAR_PLASTICITY		
Density (kg/m^3)	7850		
Young's modulus (MPa)	200000		
Poisson's ratio	0.3		
Yield stress (MPa)	528	240	
Tangent modulus (MPa)	2094	0	
Plastic strain to failure	0.07655	0.1188	
FRP material			
	Pultruded, pre-cured CFRP plate*	CFRP sheet*	GFRP sheet*
Material model	MAT_ENHANCED_COMPOSITE_DAMAGE		
Density (kg/m^3)	1740	1740	1740
Thickness per layer (mm)	1.2	1.0	0.35
Young's modulus in long. dir. (GPa)	150	69	74
Young's modulus in transverse dir. (GPa)	6.96	3.20	3.43
Longitudinal tensile strength (MPa)	2400	1034	1550
Transverse tensile strength (MPa)	240	103	155
FRP-to-concrete contact			
	Specimen SCP	Specimen SCS	Specimen SGS
Contact model	Tiebreak surface-to-surface contact		
Master surface	Concrete substrate		
Slave surface	FRP strips		
Tensile bond strength, *NFLS* (MPa)	2.57	2.57	2.57
Shear bond strength, *SFLS* (MPa)	4.58	3.24	3.24

*Average test values given by the manufacturer.

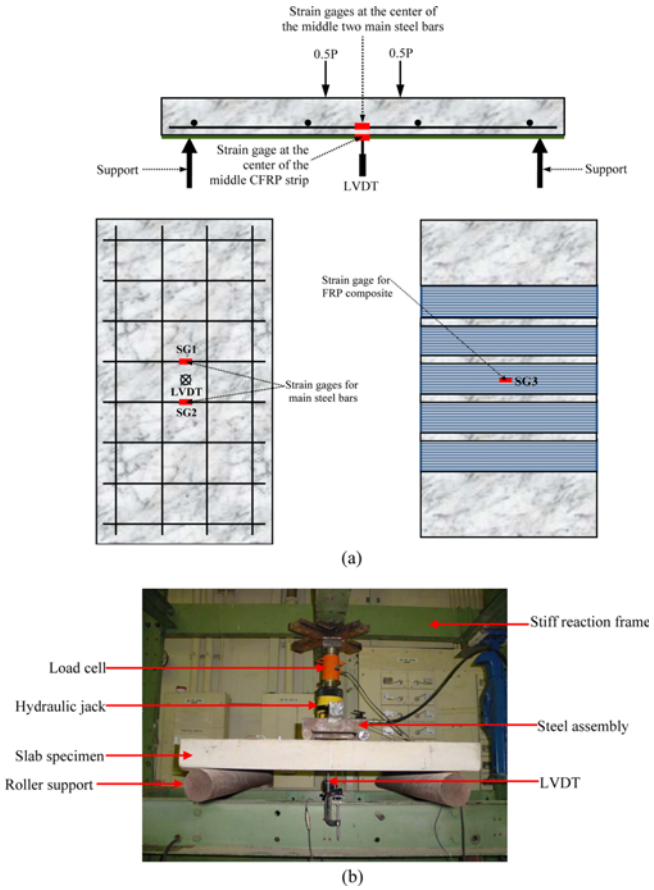

Fig. 2. Test Setup and Instrumentation: (a) Instrumentation Layout, (b) Test Setup

used in this investigation. The first system comprised of unidirectional carbon/epoxy composite fabricated in strip form using the pultrusion process; whereas, the other two systems consisted of unidirectional carbon (or E-glass)/epoxy composite fabricated using the wet lay-up process on fabric. In the first system, the prefabricated strips were bonded onto the concrete surface using epoxy adhesive. The other two systems were formed on the slabs themselves with the resin system serving both as the adhesive to the concrete and as the matrix for the FRP composite. The three FRP systems were applied to the tension surface of the slabs after sandblasting, brushing, and cleaning to ensure a substrate suitable for bonding. The average test values of the mechanical properties of the three FRP systems as given by the manufacturers are listed in Table 2.

2.3 Test Setup

Eight slabs were subjected to 4-point bending at a total span of 0.93 m and a shear span of 0.365 m. The load was applied using a 600 kN hydraulic jack connected to a stiff reaction frame. A load cell was mounted between the jack and the stiff reaction frame, as shown in Fig. 2, in order to record load during the experiment. The applied load was distributed in two lines along the width of the slab using a rigid steel assembly as illustrated in Fig. 2(b). This was done to have bending moment uniformly distributed across the slab width. As illustrated in Fig. 2, the test specimen was supported by two steel rods which acted as roller supports (restraining only the vertical movement during loading). All specimens were monotonically loaded at a displacement rate of 1 mm/min till failure. A Linear Variable Displacement Transducer (LVDT) was affixed underneath the mid-span of slabs to measure their deflection during the test. Moreover, strain gages were used to record strains at the level of main tension steel and FRP strips during the experiment. The locations of sensors are shown in Fig. 2.

3. Test Results and Discussion

Table 3 shows a summary of the flexural behavior of all test

Table 3. Experimental with FE Results with Key Points of Load-Deflection Curves for Slabs Tested in this Study*

Slab ID	Axial stiffness per unit width of FRP layers (kN/mm)	Results	P_y (kN)	P_u (kN)	Δ_y (mm)	Δ_u (mm)	K_s (kN/m)	μ_Δ	ε_{su} ($\mu\varepsilon$)	$\varepsilon_{FRP,u}$ ($\mu\varepsilon$)	Failure mode
SC	0	EXP	115.00	150.30	3.37	31.11	34163	9.24	40396	-	CC
		FE	114.12	147.49	3.15	31.36	36241	9.96	42608	-	CC
		EXP/FE	1.01	1.02	1.07	0.99	0.94	0.93	0.95	-	
SCP	180	EXP	174.80	174.80	3.56	3.56	49163	1.00	2637	3147	IC-DB
		FE	184.23	187.85	3.55	3.66	51840	1.03	2719	2988	IC-DB
		EXP/FE	0.95	0.93	1.00	0.97	0.95	0.97	0.97	1.05	
SCS	69	EXP	236.30	284.40	3.69	5.65	64103	1.53	4853	3902	IC-DB
		FE	217.59	269.55	3.70	5.23	58741	1.41	4735	4090	IC-DB
		EXP/FE	1.09	1.06	1.00	1.08	1.09	1.09	1.03	0.95	
SGS	25.9	EXP	161.8	205.2	3.95	7.79	41004	1.97	5921	7266	IC-DB
		FE	172.6	217.7	4.31	7.91	40010	1.83	6145	7429	IC-DB
		EXP/FE	0.94	0.94	0.91	0.99	1.02	1.08	0.96	0.98	

*axial stiffness per unit width of FRP layers = no. of plies of FRP × thickness of one ply of FRP × tensile modulus of FRP; P_y and Δ_y = load and mid-span deflection at yielding of main steel; P_u = ultimate load; Δ_u = mid-span deflection at ultimate; K_s = effective pre-yield stiffness; μ_Δ = deflection ductility ratio = Δ_u/Δ_y; ε_{su} = main steel strain at ultimate load; $\varepsilon_{FRP,u}$ = FRP strain at ultimate load; CC = concrete crushing; IC-DB = intermediate flexural crack induced debonding.

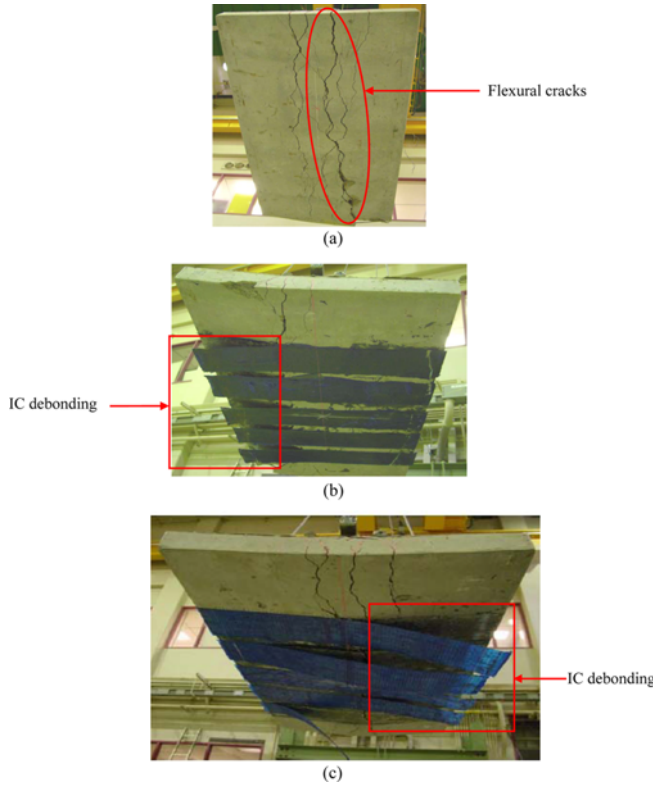

Fig. 3. Mode of Failure for Representative Samples of Test Slabs – Bottom View: (a) Control Specimen SC, (b) Strengthened Specimen SCS, (c) Strengthened Specimen SGS

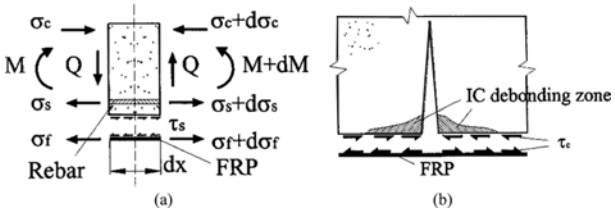

Fig. 4. Types of Interfacial Shear Stresses in FRP-strengthened RC Members (Lu *et al.*, 2007): (a) Shear Force-induced Interfacial Shear Stresses, (b) Crack-induced Interfacial Shear Stresses

groups. It should be noted that the values summarized in Table 3 are the average of the two test slabs in each group.

3.1 Modes of Failure

The final modes of failure are presented in Fig. 3 for representative samples of test specimens. The control slabs SC had a ductile flexural behavior with tension failure that was initiated by yielding of tension steel followed by concrete crushing in the compression zone. As mentioned earlier, the FRP laminates were fully extended to the end of the FRP-strengthened specimens; therefore, end debonding failure mode was mitigated and all strengthened slabs failed suddenly due to intermediate-flexural-crack-induced debonding (IC debonding). This debonding failure mode can be explained as follows:

According to Lu *et al.* (2007), the interfacial shear stresses in an FRP-strengthened RC member can be divided into two types: Those due to the shear force in the member (Fig. 4(a)) and those due to the opening-up of flexural cracks (Fig. 4(b)). Tests conducted on groups SCP, SCS and SGS showed that IC debonding was initiated under one of the two line loads. This is because at this location, both the shear force and the bending moment are at their maximum values, so both the shear force-induced interfacial shear stress and the crack-induced interfacial shear stress are maximized. Once initiated at the toe of major flexural crack under one of the two concentrated loads, the IC debonding propagated in the direction of decreasing moment towards either end of the specimen as illustrated in Figs. 3(b) and 3(c) for specimens SCS and SGS, respectively. It should be noted that a thin layer of concrete remained attached to the FRP strips upon debonding suggesting that failure occurred in the concrete rather than the interface. This may validate the proper surface preparation procedure followed during FRP installation.

3.2 Load-Deflection Curves

Load versus mid-span deflection curves are shown in Fig. 5 for all test groups. The curves shown in Fig. 5 are for one test slab of each group. As demonstrated in Fig. 5, the control group SC displayed the standard nearly-bilinear response characteristics of under-reinforced concrete flexural members. The characteristics of the load-deflection behavior of the strengthened slabs may be summarized as follows. Initially, the behavior is linear. With cracks appearing within the maximum-moment region, the load-deflection curve begins to deviate from the linear path. Once the interfacial stress near the major flexural crack reaches its critical value, the IC debonding initiates and the load drops rapidly from the peak to a significantly lower load level as depicted in Fig. 5. It should be noted that for specimen SCP, all 5 pultruded CFRP strips debonded simultaneously and the load decreased suddenly to 143 kN. For specimen SGS, the load dropped off less suddenly to 147 kN. However, for specimen SCS, the load dropped off with a stepped progression suggesting that debonding is slow rather

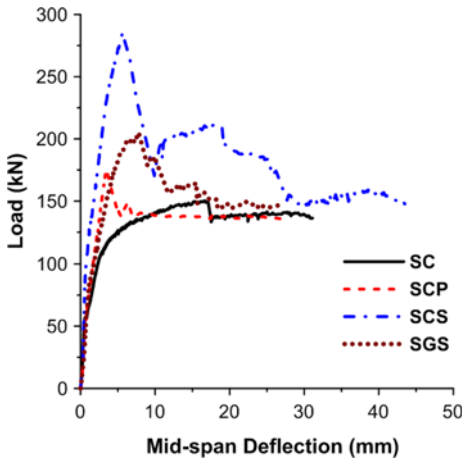

Fig. 5. Load-Deflection Curves for Test Slabs

than catastrophic. Upon reaching the peak load of 284.4 kN, three CFRP strips debonded and the load dropped off suddenly to about 170 kN but increased again to 211 kN until the other two strips debonded and the load finally dropped off to about 150 kN.

As seen from Table 3, an average gain in the flexural capacity of 16.3%, 89.2% and 36.5% was achieved for upgraded groups SCP, SCS and SGS, respectively. The lowest flexural capacity gain recorded for group SCP could be attributed to the highest axial stiffness of the CFRP pultruded plates, which resulted in early FRP debonding, compared with that for FRP wet lay-up laminates, as observed from Table 3. The test results in Table 3 also revealed that the three strengthened groups SCP, SCS and SGS had 43.9%, 87.6% and 20.0% average gain in their effective pre-yield stiffness, respectively. As the control slabs had a ductile flexural behavior, the ultimate mid-span deflection reported in Table 3 for specimen SC was calculated as the deflection corresponded to 10% reduction in the peak load. However, for FRP-strengthened specimens that failed suddenly, the ultimate mid-span deflection was taken as that corresponding to the peak load. The deflection ductility ratios summarized in Table 3 were then obtained as a ratio of the ultimate mid-span deflection to the mid-span deflection at yielding of main steel. Among the strengthened specimens, the highest deflection ductility obtained for group SGS could be attributed to the lowest axial stiffness of the GFRP wet lay-up laminates, which delayed the onset of FRP debonding, compared with that for CFRP systems as observed from Table 3. It may be generally concluded that externally bonded FRP composites are effective in terms of enhancing the flexural capacity and stiffness of RC one-way slabs. Yet, the FRP composite systems result in reduced deflection ductility.

4. Finite Element Modeling

LS-DYNA (LSTC, 2007), a general-purpose finite element program, was employed for the numerical simulation of the test slabs. The 3-D finite element model was developed using a general-purpose pre-processor FEMB. Only half of the slab was modeled accounting for its symmetry.

4.1 Model Geometry

In order to model the real behavior of tested RC slabs, it is imperative that the concrete volume be modeled using solid elements. For this reason, 8-node reduced integration solid hexahedron elements were used to model concrete volume. The main and transverse steel bars were modeled using 2-node Hughes-Liu beam elements. The externally bonded FRP composite strips were modeled using 4-node shell elements. The Belytschko-Tsay element formulation (Belytschko and Tsay, 1981) was used for shell elements.

Size of concrete solid elements ranged from 8 to 50 mm; whereas, FRP shell elements were 25 × 25 mm in size. Numerical convergence study showed that further decrease in the mesh size has little effect on the numerical results but leads to the risk of computer memory overflow and substantially increases the computing time. Fig. 6 shows the typical mesh of the upgraded slabs SCS (or SGS), which consists of 16,632 solid concrete elements, 288 beam elements for the reinforcing bars and 840 shell elements for the FRP laminates to give a total of 17,760 elements. Test results depicted that slippage of main steel bars was not noticed in any of the tested slabs as longitudinal splitting cracks were not observed (see Fig. 3). This may be attributed to the sufficient development length provided for all tension bars as they were fully extended beyond the support to the end of the specimens as depicted from Fig. 1. This observation was also confirmed from the steel strains recorded during the experiments. Consequently, the FE analysis was based on perfect bond assumption between steel bars and surrounding concrete.

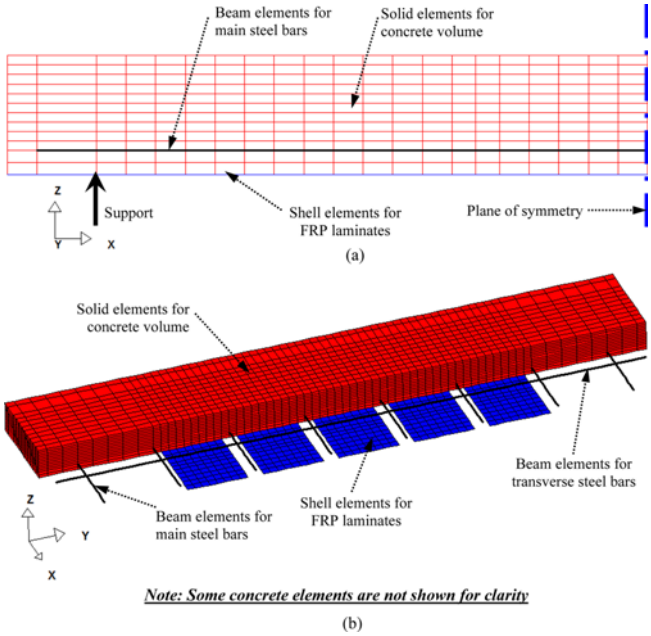

Fig. 6. Finite Element Mesh in FEMB Software showing the Modeled Components: (a) Front View, (b) Isometric View

4.2 Material Modeling

The material model type 159, MAT_CSCM_CONCRETE was employed to model the concrete volume. This is a smooth or continuous cap model available in LS-DYNA for solid elements, with a smooth intersection between the shear yield surface and the hardening cap. In this model, the initial damage surface coincides with the yield surface. Concrete cracking is considered using the traditional smeared crack approach. More details of this material model can be found in references (Murray, 2007; Murray *et al.,* 2007). The material model type 24, MAT_PIECEWISE_ LINEAR_PLASTICITY was utilized to model steel bars. This material is suited to model elasto-plastic materials with an arbitrary stress versus strain curve and an arbitrary strain rate dependency. In order to model the externally bonded FRP composite strips, the material model type MAT_054-055, MAT_ENHANCED_COMPOSITE_DAMAGE was employed. An

orthotropic material with optional brittle failure can be defined using this material card. Various failure criteria are possible for this card. The failure criterion of Chang and Chang (1987) was used in this study. The material properties used in the FE analysis is summarized in Table 2.

4.3 Erosion

The erosion option provides a way of including failure to the material models. This is not a material or physics based property; however, it lends a great means to imitate concrete spalling phenomena and produce graphical plots which are more realistic representations of the actual events. By activating this feature, the eroded solid element is physically separated from the rest of the mesh. Material failure was simulated by element erosion at a specific plastic strain; thus, whenever an element reaches this critical value, it is removed from the computation. This erosion model represents a numerical remedy to distortion, which can cause excessive and unrealistic deformation of the mesh.

The erosion option used in the FE analysis is associated with the constitutive material model. For concrete model (material model type 159), the erosion card has to be input along with the material card. The concrete elements were allowed to erode when the maximum principal strain reached 0.05 (Murray *et al.*, 2007). For other constitutive models used in the FE analysis, the erosion option is not required as the failure criteria are enough to designate material failure in the model. As previously mentioned, the failure criterion of Chang and Chang (1987) was used to define the failure of FRP laminates. For steel bars, the plastic strain to failure was enough to signify material failure.

4.4 Contact Modeling

Bond between FRP strips and concrete substrate was modeled through the tiebreak surface-to-surface contact definition of LS-DYNA. Tiebreak contact is a special type of contact. It works the same as common contact types under compressive load. The contact algorithm accounts for both normal and shear forces on the interface. Under tensile and shear loads, tiebreak allows the separation of the tied surfaces following an interface strength-based failure criterion. The following failure criterion was used in this work:

$$\left(\frac{|\sigma_n|}{NFLS}\right)^2+\left(\frac{|\sigma_s|}{SFLS}\right)^2 \geq 1 \quad (1)$$

where, σ_n is the normal stress, σ_s is the shear stress, *NFLS* is the normal failure stress and *SFLS* is the shear failure stress. After failure, this contact type behaves as a surface-to-surface contact with no thickness offsets. In addition, after failure, no interface tension is possible. In the present study, the concrete substrate was considered as master surface whereas the FRP strips were used as slave surface. The most difficult part in this contact modeling is the estimation of the failure stresses *NFLS* and *SFLS*. Improper values for *NFLS* and *SFLS* may lead to erroneous results. These failure stresses should be estimated from either pull-out testing of the two tied materials or validated empirical models. The failure stresses used in the present work were originally proposed by Lu *et al*. (2005) and then validated by Lu *et al.* (2007). These stresses can be estimated as follows:

$$NFLS = 0.395 f_{cu}^{0.55} = 0.447 (f_c^{/})^{0.55} \text{ (MPa)} \quad (2)$$

where, f_{cu} = Cube compressive strength of concrete
$f_c^{/}$ = Specified cylinder strength.

$$SFLS = 1.5 \beta_w NFLS \quad (3)$$

where, β_w is the FRP-to-concrete width ratio factor which affects the bond-slip parameters (Lu *et al*., 2005), and it is given by:

$$\beta_w = \sqrt{\frac{2.25 - b_f/b_c}{1.25 + b_f/b_c}} \quad (4)$$

where, b_c = Center-to-center spacing of FRP strips
b_f = Width of FRP strip

Values of tensile and shear bond strength, used in the FE analysis, are listed in Table 2 for FRP-strengthened slabs tested in this study. It should be noted that the contact modeling procedure followed in the FE analysis was validated in another work by Elsanadedy *et al.* (2013).

4.5 Boundary Conditions

Only half of the slab was modeled in LS-DYNA taking into account the symmetry of the slab specimens. A node set was created which consisted of nodes at support location of the slab which had to be restricted for the displacement in the global Z direction thus representing a roller support near the slab end. Symmetric boundary conditions were applied for the nodes in elements for the plane representing the continuation of the slab in reality. This included restriction of displacement in the global X direction and the rotation about the global Y and Z directions for those nodes. Since the loading was displacement controlled, another node set was created which comprised of nodes along the loading plane which were controlled to have the same Z-displacement throughout the test.

4.6 Loading Strategy

LS-DYNA uses explicit time integration algorithms for solving the problems, which are less sensitive to machine precision than other finite element solution methods. The load application process in LS-DYNA is time-history dependent. Since the testing procedure involved displacement controlled static loading, the inertia effects were removed from the dynamic equation by assigning a constant velocity to the displacement controlled node set. This will lead to zero acceleration and hence zero inertia force. The rate of change of displacement was defined as 1 mm/min to match with the experimental loading.

5. Validation of Finite Element Analysis

The validation of the FE analysis and the modeling techniques was carried out by comparing the results of the experimental

Table 4. Details of Slab Specimens Tested by other Researchers

Slab ID	Slab dimensions (mm)					f_c' (MPa)	Main tension steel		FRP properties						
	L (mm)	B (mm)	h (mm)	d (mm)	a (mm)		No. & diameter	f_y (MPa)	n	t_f (mm)	n_s	b_s (mm)	L_f (mm)	E_f (GPa)	f_{fu} (MPa)
Slabs tested by Seim *et al.* (2001)															
As-built 1	2030	480	102	83	1015	33.23	3 ∅9.5 mm	462	Control specimen						
S_{12}	2030	480	102	83	1015	33.23	3 ∅9.5 mm	462	1	1.19	2	50	1830	198	2270
S_{1m}	2030	480	102	83	1015	33.23	3 ∅9.5 mm	462	1	1.19	2	50	1460	198	2270
C_{11}	2030	480	102	83	1015	33.23	3 ∅9.5 mm	462	1	0.56	1	480	1830	77.8	835
C_{12}	2030	480	102	83	1015	33.23	3 ∅9.5 mm	462	2	0.56	1	480	1830	63.8	675
Slabs tested by Al-Rousan *et al.* (2012)															
C-1	2300	600	125	100	850	55	5 ∅12.7 mm	410	Control specimen						
G1-1	2300	600	125	100	850	55	5 ∅12.7 mm	410	2	0.165	1	600	2300	228	4275
G1-3	2300	600	125	100	850	55	5 ∅12.7 mm	410	6	0.165	3	150	2300	228	4275
G2-1	2300	600	125	100	850	55	5 ∅12.7 mm	410	1	1.2	3	100	2300	165	3030
Slabs tested by Smith *et al*. (2011)															
S1	2400	400	150	120	1000	41.36	2 ∅10 mm	566	Control specimen						
S2	2400	400	150	120	1000	41.36	2 ∅10 mm	566	3	0.166	1	100	2200	239	3163

a = shear span
B = slab width
b_s = width of FRP strip
d = effective slab depth
E_f = tensile modulus of elasticity of FRP material
f_c' = compressive strength of concrete
f_{fu} = tensile strength of FRP material
f_y = yield strength of main steel
h = slab depth
L = slab span
L_f = length of FRP strip
n = No. of plies of FRP reinforcement
n_s = No. of FRP strips
t_f = thickness of one ply of FRP reinforcement

Table 5. Experimental with FE Results with Key Points of Load-Deflection Curves for Slabs Tested by other Researchers*

Slab ID	Results	P_y (kN)	P_u (kN)	Δ_y (mm)	Δ_u (mm)	K_s (kN/m)	μ_Δ	$\varepsilon_{FRP,u}$ ($\mu\varepsilon$)	Failure mode
Slabs tested by Seim *et al.* (2001)									
As-built 1	EXP	15.30	21.80	10.88	188.02	1406	17.27	-	CC
	FE	13.96	19.26	9.02	158.00	1548	17.53	-	CC
	EXP/FE	1.10	1.13	1.21	1.19	0.91	0.99		
S_{12}	EXP	NA	42.50	NA	27.90	NA	NA	6500	IC-DB
	FE	28.01	46.43	12.79	27.27	2190	2.13	6605	IC-DB
	EXP/FE	-	0.92	-	1.02	-	-	0.98	
S_{1m}	EXP	NA	41.90	NA	28.40	NA	NA	NA	IC-DB
	FE	27.36	45.25	12.65	27.30	2162	2.16	6432	IC-DB
	EXP/FE	-	0.93	-	1.04	-	-	-	
C_{11}	EXP	NA	61.4	NA	45.70	NA	NA	NA	FR
	FE	28.3	58.4	13.82	44.20	2050	3.20	10723	FR
	EXP/FE	-	1.05	-	1.03	-	-	-	
C_{12}	EXP	NA	80.80	NA	45.73	NA	NA	NA	FSC-DB
	FE	35.97	79.28	14.79	51.35	2433	3.47	10562	FSC-DB
	EXP/FE	-	1.02	-	0.89	-	-	-	
Slabs tested by Al-Rousan *et al.* (2012)									
C-1	EXP	58.43	76.50	21.00	85.00	2783	4.05	-	CC
	FE	58.91	74.08	17.87	90.09	3296	5.04	-	CC
	EXP/FE	0.99	1.03	1.18	0.94	0.84	0.80	-	
G1-1	EXP	74.74	166.40	16.00	46.50	4672	2.91	9300	FSC-DB
	FE	89.76	177.94	16.30	57.32	5507	3.52	10257	FSC-DB
	EXP/FE	0.83	0.94	0.98	0.81	0.85	0.83	0.91	
G1-3	EXP	106.81	203.40	16.50	36.10	6473	2.19	7750	FSC-DB
	FE	126.19	215.87	17.72	39.57	7121	2.23	7035	FSC-DB
	EXP/FE	0.85	0.94	0.93	0.91	0.91	0.98	1.10	
G2-1	EXP	79.47	162.90	15.00	35.60	5298	2.37	6925	IC-DB
	FE	93.66	178.26	15.68	44.11	5973	2.81	7562	IC-DB
	EXP/FE	0.85	0.91	0.96	0.81	0.89	0.84	0.92	

Table 5. continued

Slab ID	Results	P_y (kN)	P_u (kN)	Δ_y (mm)	Δ_u (mm)	K_s (kN/m)	μ_Δ	$\varepsilon_{FRP,u}$ ($\mu\varepsilon$)	Failure mode
Slabs tested by Smith *et al.* (2011)									
S1	EXP	19.00	20.32	13.13	80.00	1447	6.09	-	CC
	FE	18.24	22.26	14.73	95.00	1238	6.45	-	CC
	EXP/FE	1.04	0.91	0.89	0.84	1.17	0.94		
S2	EXP	34.00	41.66	16.14	25.53	2107	1.58	6649	IC-DB
	FE	34.46	41.28	15.15	28.60	2275	1.89	6081	IC-DB
	EXP/FE	0.99	1.01	1.07	0.89	0.93	0.84	1.09	

*P_y and Δ_y = load and mid-span deflection at yielding of main steel; P_u = ultimate load; Δ_u = mid-span deflection at ultimate; K_s = effective pre-yield stiffness; μ_Δ = deflection ductility ratio = Δ_u/Δ_y; $\varepsilon_{FRP,u}$ = FRP strain at ultimate load; CC = concrete crushing; IC-DB = intermediate flexural crack induced debonding; FR = FRP rupture; FSC-DB = flexural-shear crack induced debonding; NA = not available data.

tests implemented in the current study and some selected studies by other researchers with the numerical results obtained from the FE model prepared in this research. In addition to the eight slabs tested in this study, another eleven one-way slab specimens tested by different researchers (Seim *et al.*, 2001; Al-Rousan *et al.,* 2012; Smith *et al.*, 2011) were used for calibrating the finite element analysis. Table 4 presents the details of the specimens, including their designation, which were selected from other studies for the purpose of validation of FE analysis. Out of the eleven specimens listed in Table 4, three were unstrengthened; whereas, eight slabs were upgraded with different FRP systems. Thus, the FE analysis was validated using the experimental database of five unstrengthened and fourteen FRP-strengthened one-way slab specimens. The experimental database used in the FE validation covers a wide range of the influencing parameters (concrete strength ranges from 24 to 55 MPa, steel reinforcement ratio ranges from 0.33 to 1% and axial stiffness per unit width of FRP layers ranges from 25.9 to 235.6 kN/mm). Summary of the experimental results of the eleven specimens tested by other studies are listed in Table 5. The following is a discussion of the FE results.

5.1 Modes of Failure

Figure 7 depicts the modes of failure for representative samples of slabs tested in this study and by other researchers as observed from the FE analysis post-processing software. The failure modes are based on contours of mid-surface maximum principal strains. For slabs tested in this study, it is noted that the failure modes predicted from the FE analysis match well with the experimental observations. From the analysis it was found that the control specimen SC failed due to concrete crushing after the formation of wide flexural cracks in the maximum-moment region, as depicted in Fig. 7(a). As presented in Figs. 7(b) and 7(c), the two strengthened slabs SCP and SCS failed suddenly due to IC debonding that initiated at the cracks where bending moments and shear forces have their maximum value then propagated in the direction of decreasing moment to the ends.

As illustrated in Table 5, the FE analysis predicted very well the failure modes for slabs tested by other researchers. For FRP-upgraded slabs, the failure was either within the maximum-moment region (FRP fracture or IC debonding) or outside the maximum-moment zone due to flexure-shear crack induced debonding. An example of FRP fracture is given in Fig. 7(d) for

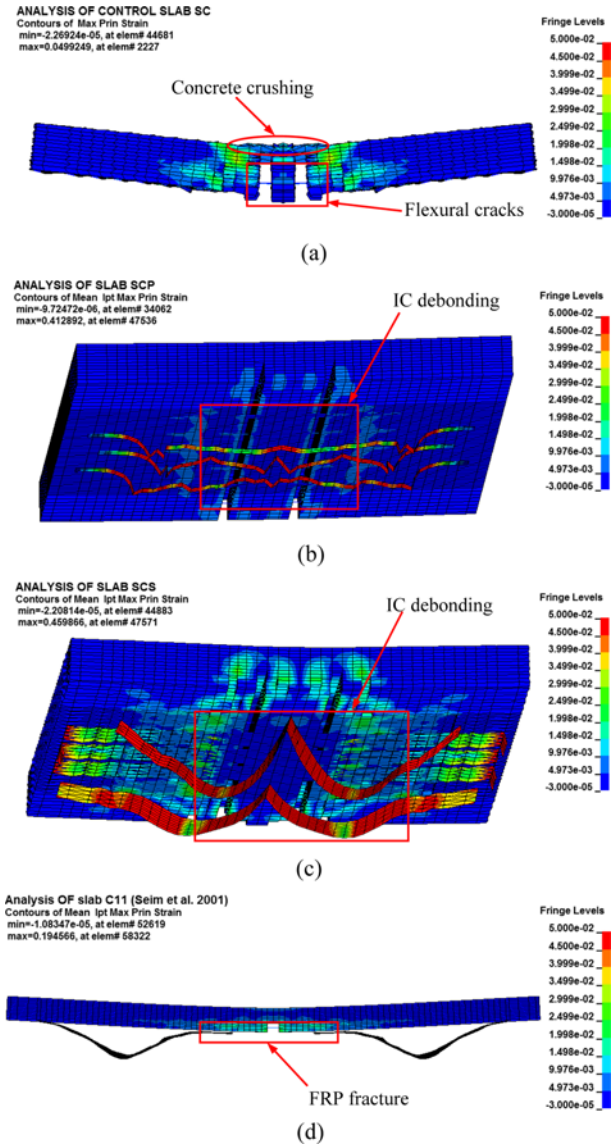

Fig. 7. FE mode of Failure for Representative Slab Samples: (a) Control Specimen SC, (b) Strengthened Specimen SCP, (c) Strengthened Specimen SCS, (d) Strengthened Specimen C_{11}

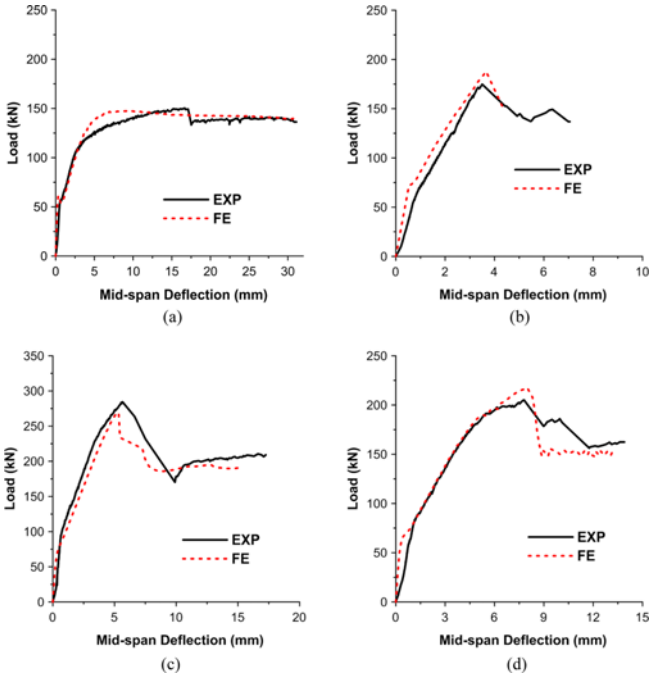

Fig. 8. Load-Deflection Comparison for Slabs Tested in this Study: (a) Specimen SC, (b) Specimen SCP, (c) Specimen SCS, (d) Specimen SGS

specimen C_{11} tested by Seim *et al.* (2001).

5.2 Load-Deflection Curves

A comparison was made between the load-deflection curves obtained from the experimental and the numerical studies for all one-way slab specimens tested in this study and by other researchers. Figs. 8 to 11 depict this comparison. As seen from the figures, the experimental load-deflection curves showed good agreement especially for the ultimate load carrying capacity, compared with the FE analysis of the control slabs as well as FRP-strengthened specimens. Tables 3 and 5 enlist the comparison details for slabs tested in this study and by other researchers, respectively. As seen from Tables 3 and 5, deviations of 1%-17% and 1%-13% were found for the numerical results for yield and ultimate loads, respectively. Yet, compared with the experimental results, deviations of 0%-21%, 1%-19% and 1%-20% were observed for mid-span deflection at yield load, mid-span deflection at ultimate load and deflection ductility, respectively. The stiffness of the slab specimens was also predicted efficiently by the FE models in comparison with the experimental results. Figs. 8 to 11 also show that the FE models were successful in imitating the softening behavior which demonstrates the accuracy of the material models. The FE analysis also revealed the effectiveness of using externally bonded FRP composite systems in upgrading the flexural capacity and stiffness of RC one-way slabs but with the reduction of their deflection ductility.

5.3 Strain Gage Results

The maximum tensile strain in the main steel obtained from

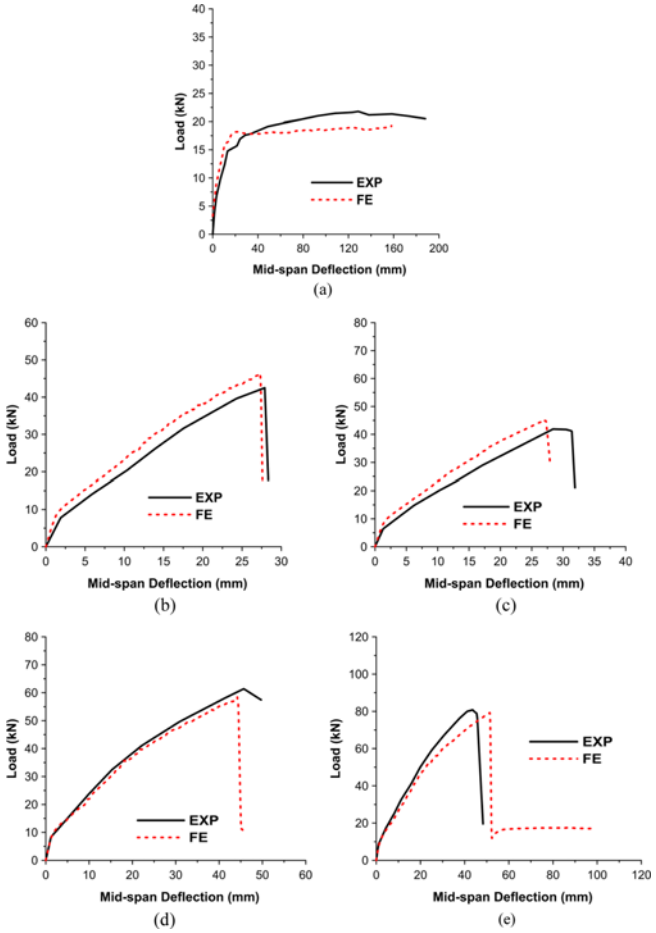

Fig. 9. Load-Deflection Comparison for Slabs Tested by Seim *et al.* (2001): (a) Specimen As-built 1, (b) Specimen S_{12}, (c) Specimen S_{1m}, (d) Specimen C_{11}, (e) Specimen C_{12}

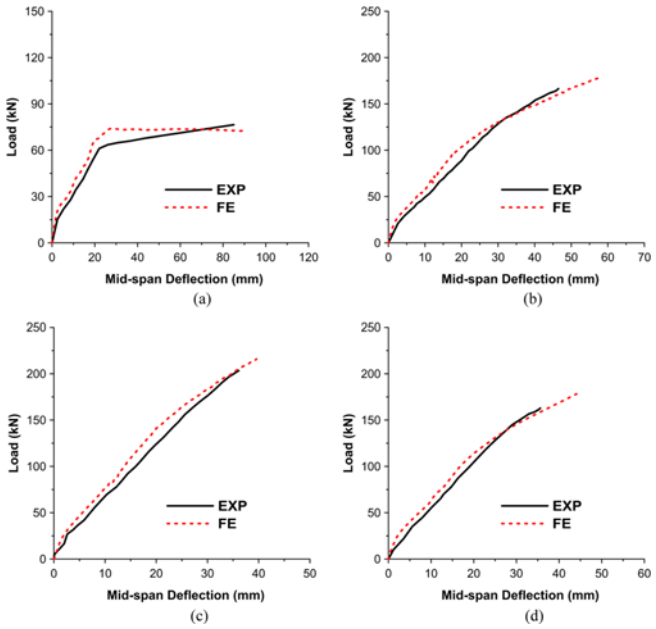

Fig. 10. Load-Deflection Comparison for Slabs Tested by Al-Rousan *et al.* (2012): (a) Specimen C-1, (b) Specimen G1-1, (c) Specimen G1-3, (d) Specimen G2-1

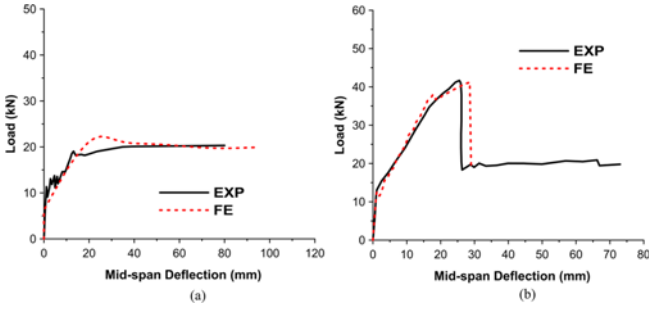

Fig. 11. Load-Deflection Comparison for Slabs Tested by Smith *et al.* (2011): (a) Specimen S1, (b)Specimen S2

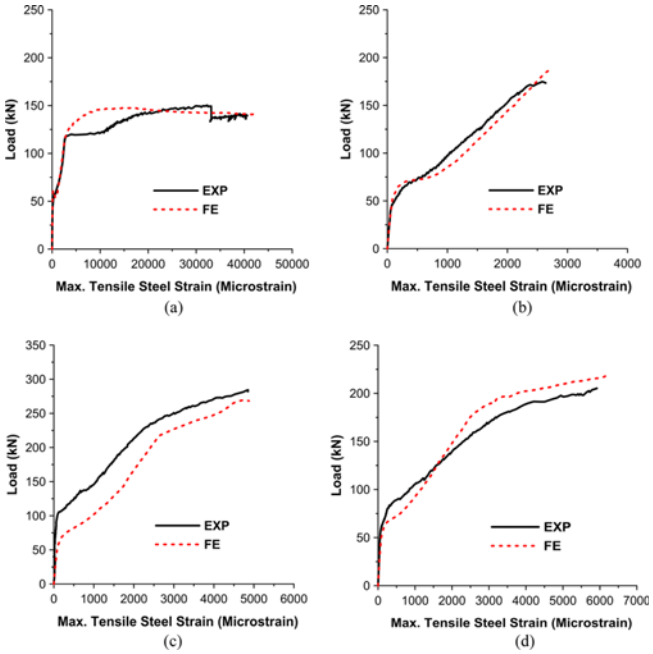

Fig. 12. Load versus Main Steel Strain Comparison for Slabs Tested in this Study: (a) Specimen SC, (b) Specimen SCP, (c) Specimen SCS, (d) Specimen SGS

the post-processing software of LS-DYNA for the tested slab specimens was compared with the experimental steel strains obtained using the strain gages. Figs. 12(a) to 12(d) depict this comparison for slabs SC, SCP, SCS and SGS, respectively. For slabs tested by other researchers, experimental steel strains were not available. Table 3 enlists measured and predicted steel strains for slab specimens tested in this study. Good agreement was achieved between the experimental and predicted steel strains. It is clear that the control slab SC had a high ductile behavior with an average strain ductility (ratio of steel strain at ultimate load to steel yield strain) of 15.3, which is typical for one-way slabs with low reinforcement ratio. Nevertheless, strain ductility of 1.0, 1.8 and 2.2 was predicted for specimens SCP, SCS and SGS, respectively.

In addition to main steel, strain gages were attached to the center of the middle FRP strips to record their strain throughout the test. Fig. 13 and Table 3 show the FRP strain comparison for

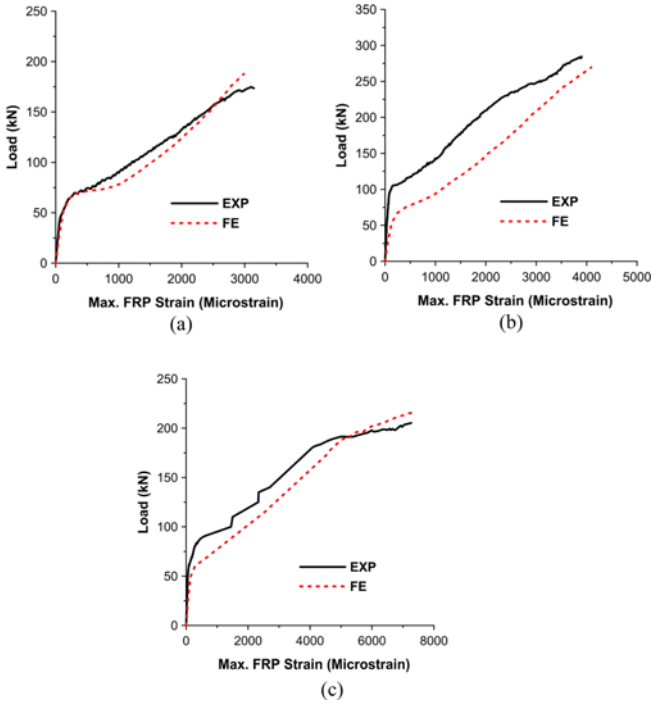

Fig. 13. Load versus FRP Strain Comparison for Upgraded Slabs Tested in this Study: (a) Specimen SCP, (b) Specimen SCS, (c) Specimen SGS

the three upgraded slabs SCP, SCS and SGS where good agreement was accomplished between the experimental and predicted values. From Table 3, it is clear that for upgraded slabs, the FRP materials did not reach their tensile capacity due to IC debonding as measured FRP strains at peak loads were 20%, 26% and 35% of their rupture strains for specimens SCP, SCS and SGS, respectively. Measured and predicted FRP strains for slab specimens tested by other researchers are listed in Table 5, in which FRP strains at peak load were available for five specimens only. Good agreement was achieved between the experimental and predicted FRP strains listed in Table 5.

6. Effect of Width and Thickness of FRP Composites

The validated FE modeling detailed previously was utilized to conduct a parametric study on the use of externally bonded FRP composite systems in the flexural upgrading of RC one-way slabs. The parameters considered in this study are both axial FRP stiffness and FRP-to-concrete width ratio. Thirteen different FRP stiffness values (ranging from very low value of 18.5 kN/mmm to high value of 370 kN/mm) with two FRP-to-concrete width ratios (ranging from 0.2 to 0.4) were numerically investigated. It should be noted that a width ratio of 1.0 was not numerically studied as it is not common in real applications. The FE matrix comprised of one control specimen S-1 and 26 FRP-strengthened specimens S-2 to S-27. Details of slabs used in the parametric study are given in Fig. 14 and Table 6. It should be noted that

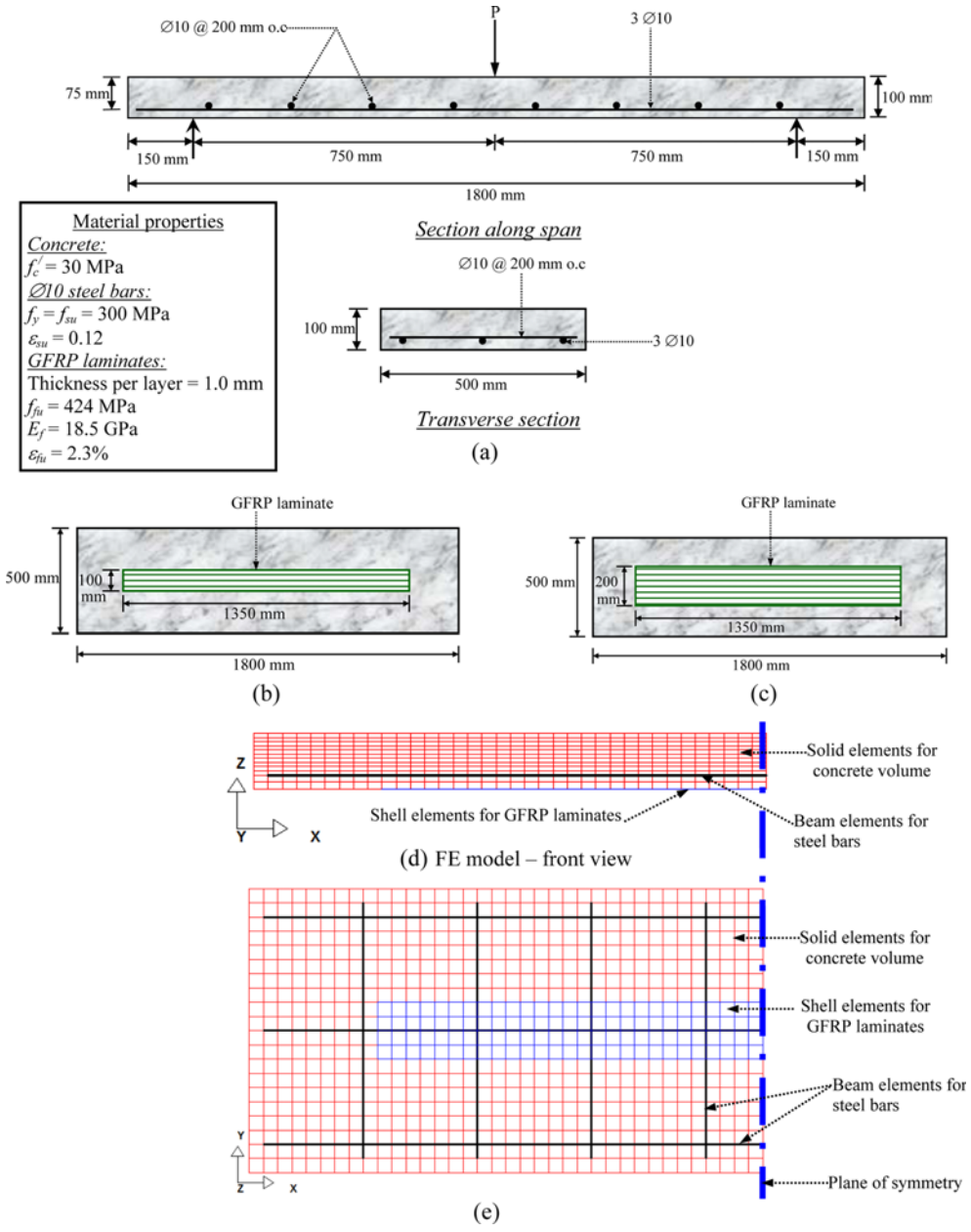

Fig. 14. Details of Slabs used in the Parametric Study: (a) Control Specimen S-1, (b) Strengthened Specimens S-2 to S-14, (c) Strengthened Specimens S-15 to S-27, (d) FE Model – Front View, (e) FE Model – Bottom View

sections of all slab specimens (S-1 to S-27) were intentionally designed to be under-reinforced with low reinforcement ratio of 0.63%. It should be also noted that in the design of FRP length for specimens S-2 to S-27, the ACI 440.2R-08 (ACI Committee 440, 2008) guidelines were followed to avoid end debonding failure mode. Summary of FE analysis results for the 27 specimens used in the parametric study is listed in Table 6. From the table, it is clear that the IC debonding is the most common failure mode for FRP-upgraded slabs. It is also evident that as the cross-sectional area of the FRP reinforcement increases, the effective pre-yield stiffness increases. Yet, both deflection ductility and FRP debonding strain get reduced. It is also noted that with the same FRP reinforcement area, increasing the FRP width is significantly more effective than increasing its thickness in terms of upgrading the flexural capacity of RC one-way slabs.

In order to study the effect of different variables on the FRP debonding strain, a new stiffness parameter (α_s) was first introduced in this study. This parameter was derived based on comprehensive regression analysis conducted on the FE results of the upgraded slabs failing by IC debonding as listed in Tables 3, 5 and 6. In this regard, FE analysis results of 29 slab specimens were used in the derivation of α_s. The stiffness parameter is a measure of the FRP stiffness with respect to concrete compressive strength and is used for estimating the FRP debonding strain in

Table 6. Details and FE Results of Slabs used in the Parametric Study*

Slab ID	FRP strengthening scheme			FE results							
	n	nt_f(mm)	b_f(mm)	P_y(kN)	P_u(kN)	Δ_y(mm)	Δ_u(mm)	K_s(kN/m)	μ_Δ	$\varepsilon_{FRP,u}$($\mu\varepsilon$)	Failure mode
S-1	Control Specimen			13.52	15.94	4.50	54.60	3005	12.1	-	CC
S-2	1	1	100	15.02	25.03	4.80	33.55	3129	7.0	22270	FR
S-3	2	2	100	19.06	35.25	5.50	48.10	3466	8.7	22703	FR
S-4	3	3	100	18.63	35.80	5.30	31.40	3515	5.9	18216	IC-DB
S-5	4	4	100	19.53	42.48	5.50	35.00	3551	6.4	15027	IC-DB
S-6	5	5	100	20.99	44.68	5.50	31.30	3817	5.7	13081	IC-DB
S-7	6	6	100	20.02	41.06	5.50	20.70	3641	3.8	9189	IC-DB
S-8	8	8	100	23.93	46.80	5.60	21.30	4274	3.8	8595	IC-DB
S-9	10	10	100	25.05	48.32	5.60	18.20	4472	3.3	7081	IC-DB
S-10	12	12	100	27.13	49.52	5.70	15.80	4759	2.8	6054	IC-DB
S-11	14	14	100	28.62	51.83	5.70	15.20	5021	2.7	5568	IC-DB
S-12	16	16	100	30.75	54.07	5.70	14.60	5394	2.6	5189	IC-DB
S-13	18	18	100	31.81	55.37	5.80	14.10	5484	2.4	4757	IC-DB
S-14	20	20	100	35.37	54.55	5.90	12.60	5994	2.1	4162	IC-DB
S-15	1	1	200	18.11	34.90	5.50	41.60	3293	7.6	22486	FR
S-16	2	2	200	21.07	53.69	5.50	57.50	3831	10.5	22865	FR
S-17	3	3	200	23.37	60.40	5.50	48.10	4248	8.7	18216	IC-DB
S-18	4	4	200	24.23	64.69	5.50	40.20	4406	7.3	14919	IC-DB
S-19	5	5	200	27.28	66.51	5.50	33.30	4960	6.1	12216	IC-DB
S-20	6	6	200	28.99	63.85	5.70	26.40	5086	4.6	9459	IC-DB
S-21	8	8	200	32.15	69.20	5.80	24.00	5544	4.1	7730	IC-DB
S-22	10	10	200	34.98	70.51	5.90	18.70	5929	3.2	5784	IC-DB
S-23	12	12	200	39.50	69.64	6.00	16.00	6584	2.7	5297	IC-DB
S-24	14	14	200	40.62	70.62	6.00	14.50	6770	2.4	4541	IC-DB
S-25	16	16	200	44.08	71.14	6.20	13.50	7109	2.2	4108	IC-DB
S-26	18	18	200	48.09	70.40	6.20	12.30	7756	2.0	3568	IC-DB
S-27	20	20	200	50.92	68.34	6.40	11.10	7956	1.7	3081	IC-DB

*n = no. of FRP layers; t_f = thickness per layer of FRP reinforcement; b_f = width of FRP laminate; P_y and Δ_y = load and mid-span deflection at yielding of main steel; P_u = ultimate load; Δ_u = mid-span deflection at ultimate; K_s = effective pre-yield stiffness; μ_Δ = deflection ductility ratio = Δ_u/Δ_y; $\varepsilon_{FRP,u}$ = FRP strain at ultimate load; CC = concrete crushing; FR = FRP rupture; IC-DB = intermediate flexural crack induced debonding.

FRP-upgraded members. This parameter is given by the following empirical formula:

$$\alpha_s = \frac{1}{\beta_w}\sqrt{\frac{nE_f t_f}{f_c'}} \tag{5}$$

where, β_w is the FRP-to-concrete width ratio factor given earlier in Eq. (4), n = Number of FRP layers, E_f = Tensile modulus of FRP reinforcement (in MPa), t_f = Thickness per layer of FRP reinforcement (in mm), and f_c' = Specified concrete strength (in MPa). It is worth mentioning that the square-root term in the right hand side of the above equation is the reciprocal of the square-root term of formula (10-2) of the ACI 440.2R-08 (ACI Committee 440, 2008) used for the estimation of FRP debonding strain in FRP-strengthened members. Additionally, this formula is a little similar to the one proposed by Chen and Teng (2001) for predicting the bond strength between FRP laminates and concrete. The relationship between the stiffness parameter (α_s) and the FRP debonding strain was plotted for the 29 debonding-controlled specimens as seen in Fig. 15. Based on FE analysis, the best-fit equation for predicting the FRP debonding strain is given by:

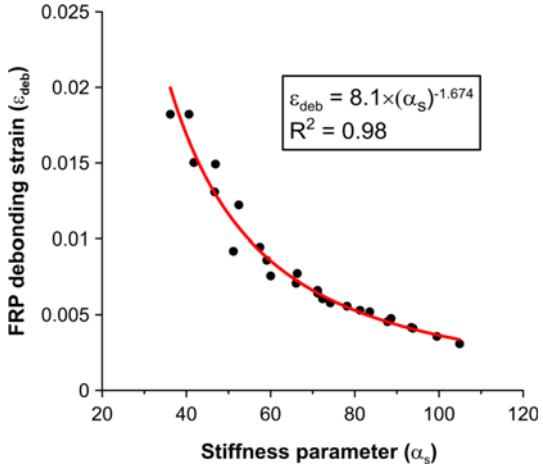

Fig. 15. Relationship between Stiffness Parameter (α_s) and FRP Debonding Strain for Upgraded Slabs (based on FE analysis)

$$\varepsilon_{deb} = 8.1(\alpha_s)^{-1.674} \tag{6}$$

The above equation has coefficient of determination (R^2) of 0.98.

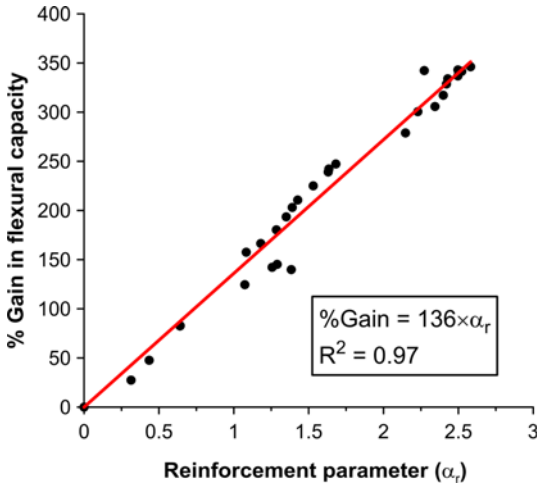

Fig. 16. Relationship between Reinforcement Parameter (α_r) and Percent Gain in Flexural Capacity for Upgraded Slabs (based on FE analysis)

In order to study the effect of FRP-strengthened slab parameters on the percent gain in flexural capacity (with respect to the unstrengthened slab), a new reinforcement parameter (α_r) was first introduced in this study. This parameter was derived based on comprehensive regression analysis conducted on the FE results of the 29 debonding-controlled FRP-upgraded slabs with respect to their corresponding control specimens. This dimensionless parameter is the ratio of the maximum allowable tensile force resisted by the FRP laminates to the yield capacity of the main tension steel bars, and is given by the following empirical equation:

$$\alpha_r = \frac{\rho_f E_f \varepsilon_{deb}}{\rho_s f_y} \tag{7}$$

where, f_y = Yield strength of main steel reinforcement
ε_{deb} = FRP debonding strain as estimated from Eq. (6)
ρ_f = FRP reinforcement ratio
ρ_s = Main steel reinforcement ratio

The FRP reinforcement ratio is given from:

$$\rho_f = \frac{A_f}{Bh} \tag{8}$$

where, A_f = Cross-sectional area of FRP reinforcement
B = Total slab width
h = Slab thickness

The relationship between the reinforcement parameter (α_r) and the percent gain in flexural capacity for the 29 debonding-controlled FRP-upgraded specimens is plotted in Fig. 16. Based on FE analysis, the best-fit equation for predicting the percent gain in flexural capacity is given by:

$$\%\text{Gain} = 136 \times \alpha_r \tag{9}$$

The R^2 value for the above equation is 0.97. It should be noted that the above proposed equations are only valid for slabs failing by either FRP rupture or IC debonding where the FRP scheme satisfies the guidelines of the ACI 440.2R-08 for the location of cutoff points for the FRP laminates. The proposed methodology cannot be applied to FRP-strengthened slabs failing by end debonding.

For FRP-upgraded slabs tested in this study and by other researchers, and failing due to either FRP rupture or IC debonding, the above proposed methodology was employed to predict their flexural capacity. The proposed methodology was then compared with the flexural capacity predictions of the ACI 440.2R-08. Since we are not dealing with a design-related problem and the goal is to predict the flexural capacity of test slabs, a strength reduction factor of one ($\phi = 1$) was utilized. Both predictions were compared with the experimental results as given in Table 7. It should be noted that in the proposed methodology, the flexural capacity of the control slabs was estimated as per the ACI 318-11 code (ACI Committee 318, 2011). From Table 7, it is noted that the proposed approach is conservative, yet accurate, with the ratio of experimental-to-predicted flexural capacity ranging from 1.0 to 1.13. The ACI 440.2R-08 predictions are non-conservative for specimens tested in this study. However, for specimens tested by other researchers, the flexural capacity estimated as per the ACI 440.2R-08 guidelines was significantly underestimated with the ratio of experimental-to-predicted flexural capacity ranging

Table 7. Proposed versus ACI 440.2R-08 Prediction of Flexural Capacity of FRP-upgraded Slabs*

Slab ID	Ultimate load (P_u) (kN)					
	EXP	PROPOSED	ACI	EXP/PROPOSED	EXP/ACI	PROPOSED/ACI
Slabs tested in this study						
SCP	174.8	172.5	176.2	1.01	0.99	0.98
SCS	284.4	268.1	322.6	1.06	0.88	0.83
SGS	205.2	202.7	225.0	1.01	0.91	0.90
Slabs tested by other researchers						
S_{12}	42.5	41.6	32.3	1.02	1.31	1.29
S_{1m}	41.9	41.6	32.3	1.01	1.30	1.29
C_{11}	61.4	54.2	44.4	1.13	1.38	1.22
G2-1	162.9	162.9	144.4	1.00	1.13	1.13
S2	41.7	40.8	34.8	1.02	1.20	1.17

*Based on strength reduction factor of one ($\phi = 1$).

from 1.13 to 1.38.

7. Conclusions

On the basis of experimental and numerical results presented in this paper, the following conclusions can be drawn:

1. Externally bonded FRP composite systems are effective in upgrading the flexural capacity and stiffness of RC one-way slabs but with the reduction of their deflection ductility.
2. Intermediate flexural crack induced debonding (IC debonding) is the most common failure mode for FRP-upgraded one-way slabs. This debonding starts at cracks where bending moments and shear forces have their maximum value then propagates in the direction of decreasing moment to the ends.
3. As the cross-sectional area of externally bonded FRP composite system increases the effective pre-yield stiffness of the one-way slab increases, however, both deflection ductility and FRP debonding strain get reduced.
4. With the same FRP reinforcement area, increasing the FRP width is significantly more effective than increasing its thickness in terms of upgrading the flexural capacity of RC one-way slabs.
5. Comparison of the finite element analysis results with the experimental results confirmed that the proposed numerical approach is appropriate for estimating the flexural capacity of both the unstrengthened and FRP-strengthened one-way slab specimens. This will thereby indicate the validity of the numerical modeling procedures, which may be used for conducting future research in the area of FRP-upgraded concrete members.
6. Based on comprehensive FE analysis conducted in this study, new stiffness and reinforcement parameters (α_s & α_r) were first introduced in this research. These parameters were employed in the establishment of two new formulas (Eqs. (6) & (9)) for predicting FRP debonding strain and percent gain of flexural capacity in FRP-strengthened RC one-way slabs. The new developed equations are only valid for slabs failing by either FRP rupture or IC debonding where the FRP scheme satisfies the guidelines of the ACI 440.2R-08 for the location of cutoff points for the FRP laminates. The proposed methodology cannot be applied to FRP-strengthened slabs failing by end debonding.
7. The proposed formulas (Eqs. (6) & (9)) were utilized to predict the ultimate load capacity for FRP-upgraded slabs tested in this study and by other researchers, and were then compared with the flexural capacity predictions of the ACI 440.2R-08. The proposed methodology was found to be conservative, yet accurate, with the ratio of experimental-to-predicted flexural capacity ranging from 1.0 to 1.13. The ACI 440.2R-08 predictions are non-conservative for specimens tested in this study. However, for specimens tested by other researchers, the flexural capacity estimated as per the ACI 440.2R-08 guidelines was significantly underestimated with the ratio of experimental-to-predicted flexural capacity ranging from 1.13 to 1.38.

Acknowledgements

The Authors would like to extend their sincere appreciation to the Deanship of Scientific Research at King Saud University for its funding of this research through the research group project No. RGP-VPP-104. Thanks are also extended to the MMB Chair for Research and Studies in Strengthening and Rehabilitation of Structures, at the Department of Civil Engineering, King Saud University for providing technical support.

References

ACI Committee 318 (2011). *Building code requirements for structural concrete and commentary*, ACI 318-11, American Concrete Institute, Detroit, MI, USA.

ACI Committee 440 (2008). *Guide for the design and construction of externally bonded FRP systems for strengthening concrete structures*, ACI 440.2R-08, American Concrete Institute, Detroit, MI, USA.

Al-Rousan, R., Issa, M., and Shabila, H. (2012). "Performance of reinforced concrete slabs strengthened with different types and configurations of CFRP." *Composites: Part B*, Vol. 43, pp. 510-521, DOI: 10.1016/j.compositesb.2011.08.050.

Aprile, A. and Feo, L. (2007). "Concrete cover rip-off of R/C beams strengthened with FRP composites." *Compos. Part B: Eng*, Vol. 38, Nos. 5-6, pp. 759-771, DOI: 10.1016/j.compositesb.2006.07.015.

Arduini, M., Di Tommaso, A., and Nanni, A. (1997). "Brittle failure in FRP plate and sheet bonded beams." *ACI Struct. J.*, Vol. 94, No. 4, pp. 363–370.

Arduini, M., Nanni, A., and Romagnolo, M. (2004). "Performance of one-way reinforced concrete slabs with externally bonded fiber-reinforced polymer strengthening." *ACI Struct. J.*, Vol. 101, No. 2, pp. 193-201.

Belytschko, T. B. and Tsay, C. S. (1981). "Explicit algorithms for nonlinear dynamics of shells." *Journal of Applied Mechanics*, Applied Mechanics Division, ASME, Vol. 48, pp. 209-231.

Buyukozturk, O. and Hearing, B. (1998). "Failure behavior of precracked concrete beams retrofitted with FRP." *J. Compos. Constr.*, ASCE, Vol. 2, No. 3, pp. 138-144, DOI: 10.1061/(ASCE)1090-0268(1998)2:3(138).

Chang, F. K. and Chang, K. Y. (1987). "A progressive damage model for laminated composites containing stress concentration." *J. Composite Materials*, Vol. 21, pp. 834-855, DOI: 10.1177/002199838702100904.

Chen, G. M., Chen, J. F., and Teng, J. G. (2012). "On the finite element modelling of RC beams shear strengthened with FRP." *Constr. & Build. Mater.*, Vol. 32, pp. 13-26, DOI: 10.1016/j.conbuildmat.2010.11.101.

Chen, J. F. and Teng, J. G. (2001). "Anchorage strength models for FRP and steel plates bonded to concrete." *J. of Struc. Eng.*, ASCE, Vol. 127, No. 7, pp. 784-791, DOI: 10.1061/(ASCE)0733-9445(2001)127:7(784).

Elsanadedy, H. M, Almusallam, T. H., Alsayed, S. H., and Al-Salloum, Y. A. (2013). "Flexural strengthening of RC beams using textile reinforced mortar – Experimental and numerical study." *Compos. Struct.*, Vol. 97, pp. 40-55, DOI: 10.1016/j.compstruct.2012.09.053.

Elsayed, W., Ebead, U. A., and Neale, K. W. (2007). "Interfacial behavior and debonding failures in FRP-strengthened concrete slabs." *J.*

Compos. Constr., ASCE, Vol. 11, No. 6, pp. 619-628, DOI: 10.1061/(ASCE)1090-0268(2007)11:6(619).

Erki, M. A. and Heffernan, P. J. (1995). "Reinforced concrete slabs externally strengthened with fiber-reinforced plastic materials." *Proc. of the 2nd Int. RILEM Symposium FRPRCS-2*, pp. 509-516.

Hu, H-T., Lin, F-M., and Jan, Y-Y. (2004). "Nonlinear finite element analysis of reinforced concrete beams strengthened by fibre-reinforced plastics." *Compos. Struct.,* Vol. 63, Nos. 3-4, pp. 271-281, DOI: 10.1016/S0263-8223(03)00174-0.

Issa, M. I., Islam, M. S., Lesile, M., Abdulla, H., and Valle, C. D. (2000). "Seismic retrofit of reinforced concrete members with CFRP composites." *Proc. of the 2nd Conf. on Seismic Repair and Rehabilitation of Structures (SRRS2)*, pp. 3-81.

Issa, M. I., Shabila, H., and Issa, M. A. (2003). "Structural behavior of reinforced concrete beams strengthened with CFRP subjected to static and fatigue loading." *Proc. of the Structural Faults and Repair Conference*, UK, 15p.

Kim, Y. J., Wight, R. G., and Green, M. F. (2008). "Flexural strengthening of RC beams with prestressed CFRP sheets: Using non-metallic anchor systems." *J. Compos. Constr.*, ASCE, Vol. 12, No. 1, pp. 44-52, DOI: 10.1061/(ASCE)1090-0268(2008)12:1(44).

Lesmana, C. and Hu, H-T. (2014). "Parametric analyses of square reinforced concrete slabs strengthened by fiber-reinforced plastics." *Constr. & Build. Mater.*, Vol. 53, pp. 294-304, DOI: 10.1016/j.conbuildmat.2013.11.083.

Livermore Software Technology Corporation (LSTC) (2007). *LS-DYNA user's keyword manual (nonlinear dynamic analysis of structures in three dimensions)*: *Volume 1*, Version 971, LSTC, Livermore, California, USA.

Lu, X. Z., Teng, J. G., Ye, L. P., and Jiang, J. J. (2005). "Bond-slip models for sheets/plates bonded to concrete." *Eng. Struc.*, Vol. 27, No. 6, pp. 920-937, DOI: 10.1016/j.engstruct.2005.01.014.

Lu, X. Z., Teng, J. G., Ye, L. P., and Jiang, J. J. (2007). "Intermediate crack debonding in FRP-strengthened RC beams: FE analysis and strength model." *J. Compos. Constr.*, ASCE, Vol. 11, pp. 161-174, DOI: 10.1061/(ASCE)1090-0268(2007)11:2(161).

Lundquist, J., Nordin, H., Täljsten, B., and Olafsson, T. (2005). "Numerical analysis of concrete beams strengthened with CFRP – A study of anchorage lengths." In: FRP in Construction, *Proc. of the Int. Symp. of Bond Behaviour of FRP in Structures*, pp. 247-254.

Mazzotti, C., Savoia, M., and Ferracuti, B. (2008). "An experimental study on delamination of FRP plates bonded to concrete." *Constr. & Build. Mater.*, Vol. 22, pp. 1409-1421, DOI: 10.1016/j.conbuildmat.2007.04.009.

Meier, U. (1992). "Carbon fiber-reinforced polymers: Modern materials in bridge engineering." *Struct. Eng. Int.*, Vol. 92, No. 1, pp. 7-12, DOI: 10.2749/101686692780617020.

Meier, U. (1995). "Strengthening of structures using carbon fibre/epoxy composites." *Constr. & Build. Mater.*, Vol. 9, No. 6, pp. 341–351, DOI: 10.1016/0950-0618(95)00071-2.

Mosallam, A. S. and Mosalam, K. M. (2003). "Strengthening of two-way concrete slabs with FRP composite laminates." *Constr. & Build. Mater.*, Vol. 17, pp. 43-54, DOI: 10.1016/S0950-0618(02)00092-2.

Murray, Y. D. (2007). *User's manual for LS-DYNA concrete material model 159*, Report No. FHWA-HRT-05-062, US Department of Transportation, Federal Highway Administration National Transportation Systems Center, USA.

Murray, Y. D., Abu-Odeh, A., and Bligh, R. (2007). *Evaluation of concrete material model 159*, Report No. FHWA-HRT-05-063, US Department of Transportation, Federal Highway Administration National Transportation Systems Center, USA.

Norris, T., Saadatmanesh, H., and Ehsani, M. R. (1997). "Shear and flexural strengthening of R/C beams with carbon fiber sheets." *J. Struct. Eng.*, ASCE, Vol. 123, No. 7, pp. 903-11, DOI: 10.1061/(ASCE)0733-9445(1997)123:7(903).

Obaidat, Y. T., Heyden, S., and Dahlblom, O. (2010). "The effect of CFRP and CFRP/concrete interface models when modeling retrofitted RC beams with FEM." *Compos. Struct.,* Vol. 92, pp. 1391-1398, DOI: 10.1016/j.compstruct.2009.11.008.

Oehlers, D. J., Park, S. M., and Ali, M. S. M. (2003). "A structural engineering approach to adhesive bonding longitudinal plates to RC beams and slabs." *Composites Part A*, Vol. 34, pp. 887-897, DOI: 10.1016/S1359-835X(03)00153-2.

Santhakumar, R., Chandrasekaran, E., and Dhanaraj, R. (2004). "Analysis of retrofitted reinforced concrete shear beams using carbon fibre composite." *Electron. J. Struct. Eng.*, Vol. 4, pp. 66-74.

Sebastian, W. M. (2001). "Significance of midspan debonding failure in FRP-plated concrete beams." *J. Struct. Eng.*, ASCE, Vol. 127, No. 7, pp. 792-798, DOI: 10.1061/(ASCE)0733-9445(2001)127:7(792).

Seim, W., Horman, M., Karbhari, V., and Seible, F. (2001). "External FRP poststrengthening of scaled concrete slabs." *J. Compos. Constr.*, ASCE, Vol. 5, pp. 67-75, DOI: 10.1061/(ASCE)1090-0268(2001) 5:2(67).

Shahway, M., Beitelman, T., Arockiasamy, M., and Sowrirajan, R. (2001). "Flexural strengthening with carbon fiber-reinforced polymer composites of preloaded full-scale girders." *ACI Struct. J.*, Vol. 98, No. 5, pp. 735-742.

Smith, S.T. and Teng, J.G. (2001). "Interfacial stresses in plate beams." *Eng. Struct.*, Vol. 23, No. 7, pp. 857-571, DOI: 10.1016/S0141-0296(00)00090-0.

Smith, S. T., Hu, S., Kim, S. J., and Seracino, R. (2011). "FRP-strengthened RC slabs anchored with FRP anchors." *Eng. Struct.*, Vol. 33, No. 4, pp. 1075-1087, DOI: 10.1016/j.engstruct.2010.11.018.

Tan, K. Y. (2003). *Evaluation of externally bonded CFRP systems for the strengthening of RC slabs*, MSc Thesis, University of Missouri-Rolla, 141p.